Research Letter DOI: 10.15541/jim20240125

Predicting the Degradability of Bioceramics through a DFT-based Descriptor

CHEN Mengjie[1,2], WANG Qianqian[1,2], WU Chengtie[1,2], HUANG Jian[1,2,3]

(1. State Key Laboratory of High Performance Ceramics and Superfine Microstructure, Shanghai Institute of Ceramics, Chinese Academy of Sciences, Shanghai 200050, China; 2. Center of Materials Science and Optoelectronics Engineering, University of Chinese Academy of Sciences, Beijing 100049, China; 3. Materials Genome Institute, Shanghai University, Shanghai 200444, China)

Abstract: Bioceramics have attracted extensive attention for bone defect repair due to their excellent bioactivity and degradability. However, challenges remain in matching the rate between bioceramic degradation and new bone formation, necessitating a deeper understanding of their degradation properties. In this study, density functional theory (DFT) calculations was employed to explore the structural and electronic characteristics of silicate bioceramics. These findings reveal a linear correlation between the maximum isosurface value of the valence band maximum (VBM_{Fmax}) and the degradability of silicate bioceramics. This correlation was subsequently validated through degradation experiments. Furthermore, the investigation on phosphate bioceramics demonstrates the potential of this descriptor in predicting the degradability of a broader range of bioceramics. This discovery offers valuable insights into the degradation mechanism of bioceramics and holds promise for accelerating the design and development of bioceramics with controllable degradation.

Key words: bioceramics; silicate; phosphate; first principles; degradation

During the past decades, bioceramics have drawn huge attention as promising biomaterials for bone tissue regeneration[1]. Early bioceramics, such as alumina and zirconia, exhibited good chemical stability, corrosion resistance and a porous three-dimensional structure that benefit for bone defect repair. However, these materials have the disadvantages of immune rejection and low biological activity within the human body, hindering their clinical application[2]. With the development of materials sciences, numerous materials have emerged as bone substitutes, including hydroxyapatite (HAP, $Ca_{10}(PO_4)_6(OH)_2$)[3], calcium phosphate[4] and bioactive glasses[5]. And the latest third generation biomaterials, such as silicate bioceramics, are bioactive with the capacity to release Si ions and form a bone-like apatite layer. These biomaterials can promote specific cellular responses at the molecular level so that they could stimulate the regeneration of tissue[6]. The ideal materials for bone tissue regeneration should possess high bioactivity and biodegradability as their major beneficial characteristics[7].

As the biomaterials gradually degrade, new bone tissues begin to repair and replace the damaged ones, leading to the growth of a completely new bone. These bone tissues repairing materials are capable of forming a chemically stable interface with surrounding tissues by developing a bone-like apatite on their surface[8]. The process of apatite formation can be controlled *in vitro* by adjusting the chemical composition of the biomaterials. Due to the ability to stimulate bone regeneration and mimic the biological tissue, bioceramics have been widely developed by causing body respond as if it was in the presence of natural tissue[9]. Studies have demonstrated that the Ca and Si ions released from silicate bioceramics can stimulate and enhance cells proliferation and differentiation *in vitro*[10-11]. Moreover, many specific ions (*e.g.* Sr^{2+}, Cu^{2+}, Mg^{2+}, and Zn^{2+}) have been incorporated within silicate bioceramics to overcome the limitations of original silicate-based biomaterials[9]. A comparative study by Ma *et al*. on the degradation and apatite formation of magnesium and zinc incorporated calcium silicate found that the inclusion of these

Received date: 2024-03-14; **Revised date:** 2024-05-04; **Published online:** 2024-05-16
Foundation item: National Key Research and Development Program of China (2023YFB3813000); National Natural Science Foundation of China (52272256); State Key Laboratory of Advanced Technology for Materials Synthesis and Processing (Wuhan University of Technology) (2022-KF-77)
Biography: CHEN Mengjie (1998–), male, Master candidate. E-mail: chenmengjie20@mails.ucas.ac.cn
陈梦杰(1998–), 男, 硕士研究生. E-mail: chenmengjie20@mails.ucas.ac.cn
Corresponding author: HUANG Jian, professor. E-mail: huangj@shu.edu.cn
黄 健, 研究员. E-mail: huangj@shu.edu.cn

elements offers an effective way to modulate degradation and apatite formation of Ca-Si-based bioceramics[12].

Silicate bioceramics have been widely studied in recent decades because of their excellent bioactivity[13], super biocompatibility[14] and fast degradability[15] in comparison with HAP and phosphate-based bioceramics. These materials have a broad range of chemical compositions, enabling the tuning of their physical, chemical and biological properties to satisfy the requirements of tissue regeneration[1]. While silicate bioceramics exhibit a faster degradation rate compared to phosphate-based bioceramics, this rate can be tailored to align with the desired rate of new bone formation[16]. In order to develop more innovative and effective silicate bioceramics, researchers have improved the biodegradability of silicate bioceramics by adjusting their mechanical properties[17], incorporating the other biomaterials[18] and introducing doping ions[19]. However, the study remains limited from the view of theoretical calculation. In this study, a relationship between electronic structure of materials and biodegradability was investigated, and a suitable descriptor utilizing computational modeling was found. In addition, degradation experiments were designed to verify the accuracy of this descriptor. It can serve as a powerful tool to better understand the degradation mechanism of silicate bioceramics *in vivo*, which is crucial for evaluating material biocompatibility and lays a foundation for the design and development of novel hard tissue materials[20].

1 Materials and methods

1.1 First principles calculations

All calculations were performed at the density functional theory (DFT) conducted by the Vienna *ab initio* simulation package (VASP)[21]. The projector augmented wave (PAW) method and plane-wave basis set were used[22-23]. The Perdew-Burke-Ernzerhof (PBE) generalized gradient approximation (GGA) was adopted to treat exchange-correlation effects in the form of the PBE function[24]. The cut-off energy for the plane-wave basis was set to 520 eV. The optimization procedure was repeated until the average energy and force change were less than 1.0×10^{-6} eV/atom and 0.01 eV/Å, respectively. For atomic relaxation calculations, meshs of k points were generated using the Monkhorst-Pack scheme to sample the Brillouin zone[25]. The crystal structures were found in inorganic crystal structure database (ICSD). Visualizations of the charge density of valence band maximum (VBM) of silicate bioceramics are performed using VESTA software[26].

1.2 Degradation experiments

Akermanite ($Ca_2MgSi_2O_7$), hardystonite ($Ca_2ZnSi_2O_7$), bredigite ($Ca_7MgSi_4O_{16}$) and β-calcium silicate (β-$CaSiO_3$) powders were purchased from Kunshan Chinese Technology New Materials Co., Ltd (China). The powders were milled at 500 r/min for 12 h and sieved through a 63 μm (250-mesh) sieve. Tris-HCl solution (Tris-(hydroxymethyl)-aminomethane and HCl, 0.01 mol/L, pH 7.4) was used as immersion medium for degradation tests. The obtained powders were soaked into Tris-HCl solution (pH 7.4) for 7, 14, 21 and 28 d with the ratio of the solution volume to powders weight was 200 mL/g. The solutions were put into a shaker with the temperature of 37 ℃ and the shaking frequency of 100 r/min. The immersion medium was refreshed and the powders were dried at 120 ℃ for 6 h and weighed at every time point. Five samples were selected in each group.

2 Results and discussion

2.1 Structure and properties of the silicate bioceramics

A variety of silicate bioceramics, including $CaSiO_3$, Ca_2SiO_4, Ca_3SiO_5, and so on, were selected for analysis and comparison. The calculated lattice parameters of these silicate bioceramics are compared with experimental values in Table S1, and the 1% disagreement suggests that the optimized structures are reasonable.

These silicate bioceramics exhibit diverse chemical compositions and crystal structures. Multiple factors, including chemical element composition, crystal structure and porosity, affect the degradation of materials[27]. The degradation of bioceramics is a complex process of competition among many factors. Typically, the porosity affects the degradation of the material, and the porous structures tend to degrade more rapidly. Therefore, the relationship between porosity and degradation of bioceramics was considered. Previous studies[12, 28] have proved that the degradability of $CaSiO_3$ is greater than that of Ca_2SiO_4, and the calculations also show that the porosity (void space) of $CaSiO_3$ (58.03%) was greater than that of Ca_2SiO_4 (57.19%). However, despite having a porosity of 57.30%, $Ca_2MgSi_2O_7$ degrades more rapidly than $Ca_2ZnSi_2O_7$, whose porosity stands at 57.87%. From this point of view, the void space does not follow a clear trend in determining the degradation of bioceramics. Similarly, no obvious rules emerge when comparing the density with degradation of these materials. Therefore, more detailed calculations are needed to elucidate the intricate relationship between the degradation of bioceramics and their physicochemical properties.

2.2 Valence band maximum (VBM) of the silicate bioceramics

The chemical reactivity can be related to the highest occupied molecular orbital (HOMO) and lowest unoccupied molecular orbital (LUMO) characteristics in molecules, whereas in bulk materials, it can be described by the valence band maximum (VBM) and the conduction band minimum (CBM)[29-30]. Previously, the hydration sensitivity of triclinic tricalcium silicate was investigated by a combination of DFT calculations and molecular dynamics[31]. It was found that the long-term reaction with water molecules is governed by the proton transport of silicate, which is intrinsically linked to the VBM of the bulk solid. Similarly, during the degradation of bioceramics, there is a process of ion precipitation and exchange that leads to the formation of a bone-like apatite layer (Fig. 1). And this ion-exchange process is similar to the proton transport in long-term reaction with water molecules. Therefore, it was postulated that the VBM of the bulk solid could serve as a descriptor to estimate the degradation of bioceramics.

The partial charge density at VBM was obtained to characterize the differences of the electronic structure of silicate bioceramics. The VBM of $CaSiO_3$, $Ca_2ZnSi_2O_7$, Zn_2SiO_4 are shown in Fig. 2. In previous studies[12, 28], the degradability of these three silicate bioceramics are in descending order of $CaSiO_3$, $Ca_2ZnSi_2O_7$ and Zn_2SiO_4. In $CaSiO_3$, the charge density was primarily distributed around O atom, with some regions exhibiting particularly high density. In contrast, the charge density in $Ca_2ZnSi_2O_7$ is distributed around the Zn atom, although the extent of this distribution is smaller than that observed in $Ca_2MgSi_2O_7$. Finally, the charge density in the Zn_2SiO_4 is once again primarily distributed around O atom.

Therefore, the maximum isosurface value of the valence band maximum (VBM_{Fmax}) of a total of 20 silicate bioceramics were collected, aiming to establish a connection with their degradability. As depicted in Fig. 3, the VBM_{Fmax} values of these silicate bioceramics were arranged from the highest to the lowest, which generally mirrored the order of their mineralization ability, ranging from the strongest to the weakest, as outlined in Table 1[32]. In general, the mineralization of bioceramics is a complex process including degradation and precipitation, which inspires us to further explore the relationship between VBM_{Fmax} and the degradability of bioceramics.

In order to include as many bioceramics as possible, the 7-day ion release value in simulated body fluid (SBF) and the 28-day weight loss value in Tris-HCl were selected from previous literatures (Table S2)[10, 12, 33-54]. By considering the overall maximum ion release, weight loss and the value of VBM_{Fmax} for each silicate bioceramics, a primarily linear relationship among these factors was observed. However, these experimental values were extracted from different research groups, which may introduce some disagreements. Thus, the linear correlation was further corroborated by a degradation experiments (Fig. 4). From Fig. 4, it is evident that as the ions release and weight loss increases, VBM_{Fmax} increases. As a result, it can be confidently concluded that, the degradability of silicate bioceramics exhibits a linear correlation with VBM_{Fmax}, indicating that VBM_{Fmax} serves as a reliable descriptor for characterizing the degradability of silicate bioceramics.

2.3 Valence band maximum (VBM) of the phosphate bioceramics

On this basis, calculations and analysis were further extended to phosphate bioceramics. Phosphate bioceramics[55], including hydroxyapatite (HAP), tricalcium phosphate (TCP) and their mixture bidirectional calcium phosphate (BCP), are widely used bioactive ceramic materials. Phosphate bioceramics have similar chemical composition to human bone mineralization, and they possess good biocompatibility and excellent osteogenic conductivity, making them highly regarded as ideal bone repair or biological replacement materials[32,56-57]. During degradation, these materials release bioactive ions such as Ca^{2+} and PO_4^{3-}, which not only stimulate osteogenic differentiation of cells but also induce bone formation[58]. Similar to the *in vivo* degradation of silicate bioceramics mentioned above, these active ions can also form bone-like apatite precipitates on the surface of ceramic materials[59].

Therefore, multiple phosphate bioceramics were further chosen for computational analysis. Corresponding data for the degradation of these phosphate bioceramics can be found in Table S3[53, 60]. Degradability of these phosphate bioceramics is much lower than those of silicate bioceramics, where solubility was usually used to describe the degradation. The structures of these phosphate bioceramics were optimized (Table S4), and it was observed that the calculated unit cell parameters closely aligned with the structures from ICSD.

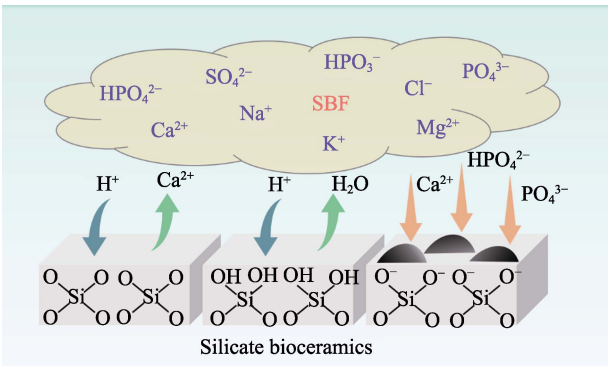

Fig. 1　Bone-like apatite layer formed after degradation of silicate bioceramics
SBF: simulated body fluid

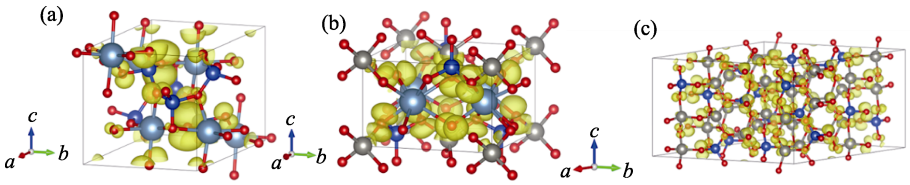

Fig. 2 Valence band maximum (VBM) of silicate bioceramics
(a) $CaSiO_3$; (b) $Ca_2ZnSi_2O_7$; (c) Zn_2SiO_4. The isosurface level is set at 0.002 e/Å^3

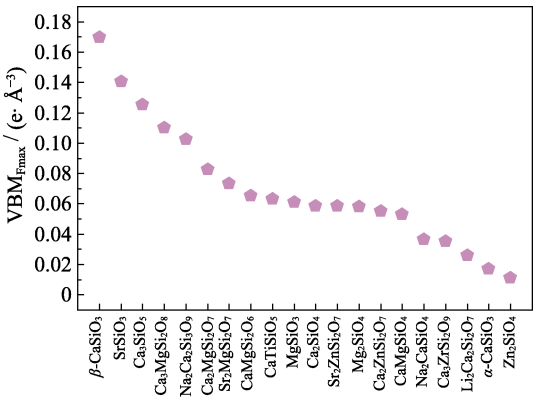

Fig. 3 VBM$_{Fmax}$ of silicate bioceramics

Based on the previous analysis of the degradation performance of silicate bioceramics, a correlation between the VBM$_{Fmax}$ and their degradation characteristics was established. Extending this descriptor to phosphate bioceramics, the VBM$_{Fmax}$ of phosphate bioceramics was also calculated and plotted against the degradation data.

Table 1 Apatite-mineralization ability of silicate bioceramics[32]

Name	Chemical formula	Mineralization ability
Wollastonite	$CaSiO_3$	▲▲▲▲*
Dicalcium silicate	Ca_2SiO_4	▲▲▲▲
Tricalcium silicate	Ca_3SiO_5	▲▲▲▲
Akermanite	$Ca_2MgSi_2O_7$	▲▲▲
Merrwinite	$Ca_3MgSi_2O_8$	▲▲▲
Diopside	$CaMgSi_2O_6$	▲▲
Monticellite	$CaMgSiO_4$	▲▲
Baghdadite	$Ca_3ZrSi_2O_9$	▲▲
Dimagnesium silicate	Mg_2SiO_4	▲
Magnesium silicate	$MgSiO_3$	▲
Zinc silicate	Zn_2SiO_4	▲
Hardystonite	$Ca_2ZnSi_2O_7$	▲
Sphene	$CaTiSiO_5$	▲
Strontium-akermanite	$Sr_2MgSi_2O_7$	▲
Strontium-hardystonite	$Sr_2ZnSi_2O_7$	▲

*▲▲▲▲: Extra strong; ▲▲▲: Strong; ▲▲: Average; ▲: Weak

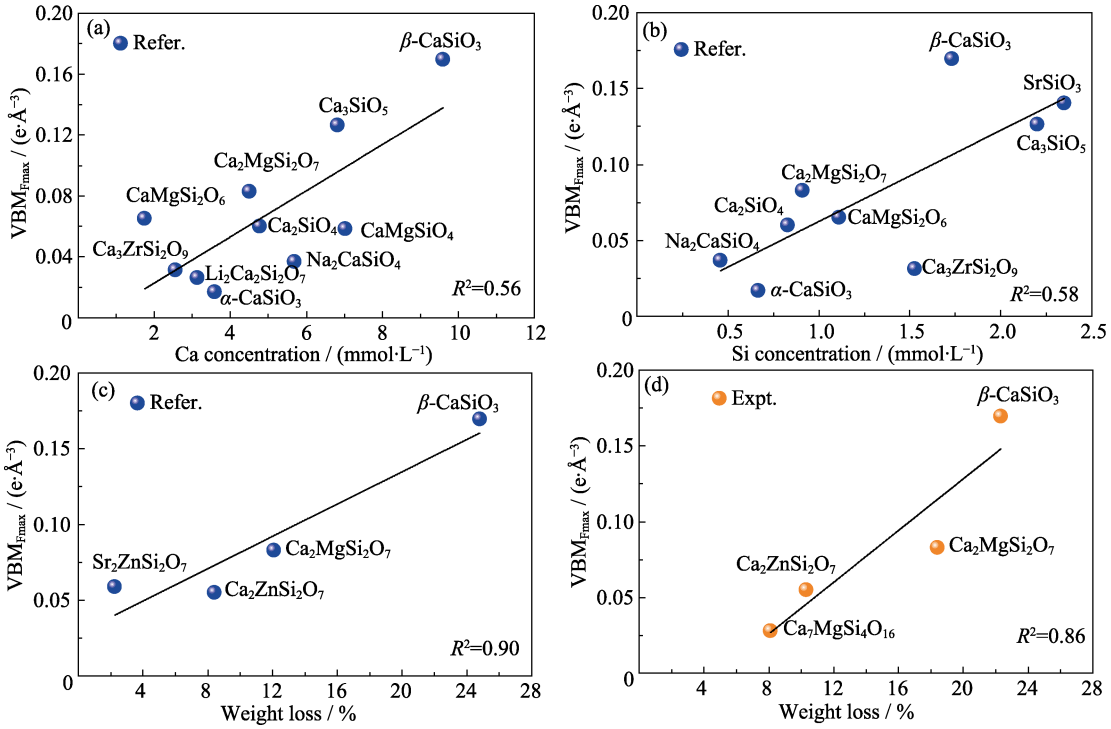

Fig. 4 Linear relationships between VBM$_{Fmax}$ and the degradation value of silicate bioceramics
7-day ion release values of (a) Ca and (b) Si in simulated body fluid (SBF); 28-day weight loss values in (c) Tris-HCl from references and (d) Tris-HCl from the degradation experiments

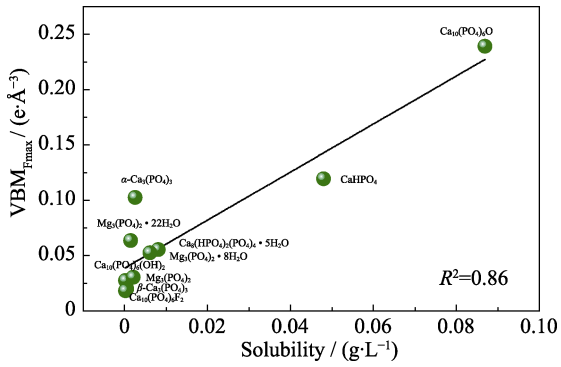

Fig. 5　Linear relationship between VBM_{Fmax} and solubility of phosphate bioceramics

It can be seen from Fig. 5 that the data points in the figure basically show a linear relationship, indicating the degradability of phosphate bioceramics increases with the increase of its VBM_{Fmax}. Therefore, it can be concluded that, similarly to silicate bioceramics, the VBM_{Fmax} of phosphate bioceramics also serves as a reliable descriptor of its degradability. In addition, for zirconia exhibiting low biological activity, the analyzed VBM_{Fmax} approaches zero, further confirming the wide adaptability of the descriptor.

3　Conclusions

The degradability of bioceramics, particularly focusing on silicate and phosphate varieties, was investigated using first principles calculations combined with experimental tests. Analysis of the electronic structure of bioceramics indicated an intriguing correlation between VBM and degradability. Specifically, a linear relationship between the VBM_{Fmax} and the degradation of the bioceramics was observed, which was further validated through the degradation experiments. Based on these findings, it is proposed that VBM_{Fmax} can serve as a reliable descriptor for characterizing the degradability of bioceramics. Overall, these findings not only enhance understanding of the degradation mechanisms of these materials, but also lay a foundation for the design and development of bioceramics with controllable degradation.

Supporting materials

Supporting materials related to this article can be found at https://doi.org/10.15541/jim20240125.

References:

[1] WU C T, CHANG J. A review of bioactive silicate ceramics. *Biomedical Materials*, 2013, **8(3):** 12.

[2] KANG Z R, YU B, FU S Y, *et al.* Three-dimensional printing of $CaTiO_3$ incorporated porous β-Ca_2SO_4 composite scaffolds for bone regeneration. *Applied Materials Today*, 2019, **16:** 132.

[3] MOHAN N, PALANGADAN R, FERNANDEZ F B, *et al.* Preparation of hydroxyapatite porous scaffold from a 'coral-like' synthetic inorganic precursor for use as a bone substitute and a drug delivery vehicle. *Materials Science and Engineering: C*, 2018, **92:** 329.

[4] MEISSNER R, BERTOL L, REHMAN M A U, *et al.* Bioprinted 3D calcium phosphate scaffolds with gentamicin releasing capability. *Ceramics International*, 2019, **45(6):** 7090.

[5] ERASMUS E P, SULE R, JOHNSON O T, *et al. In vitro* evaluation of porous borosilicate, borophosphate and phosphate bioactive glasses scaffolds fabricated using foaming agent for bone regeneration. *Scientific Reports*, 2018, **8:** 13.

[6] SRINATH P, AZEEM P A, REDDY K V. Review on calcium silicate-based bioceramics in bone tissue engineering. *International Journal of Applied Ceramic Technology*, 2020, **17(5):** 2450.

[7] JODATI H, YILMAZ B, EVIS Z. Calcium zirconium silicate (baghdadite) ceramic as a biomaterial. *Ceramics International*, 2020, **46(14):** 21902.

[8] RIBAS R G, SCHATKOSKI V M, MONTANHEIRO T L D, *et al.* Current advances in bone tissue engineering concerning ceramic and bioglass scaffolds: a review. *Ceramics International*, 2019, **45(17):** 21051.

[9] SCHATKOSKI V M, MONTANHEIRO T L D, DE MENEZES B R C, *et al.* Current advances concerning the most cited metal ions doped bioceramics and silicate-based bioactive glasses for bone tissue engineering. *Ceramics International*, 2021, **47(3):** 2999.

[10] WU C, CHANG J. Degradation, bioactivity, and cytocompatibility of diopside, akermanite, and bredigite ceramics. *Journal of Biomedical Materials Research Part B: Applied Biomaterials*, 2007, **83B(1):** 153.

[11] SUN H L, WU C T, DAI K R, *et al.* Proliferation and osteoblastic differentiation of human bone marrow-derived stromal cells on akermanite-bioactive ceramics. *Biomaterials*, 2006, **27(33):** 5651.

[12] MA J, WANG C Z, HUANG B X, *et al. In vitro* degradation and apatite formation of magnesium and zinc incorporated calcium silicate prepared by Sol-Gel method. *Materials Technology*, 2021, **36(7):** 420.

[13] CHEN Y W, HO C C, HUANG T H, *et al.* The ionic products from mineral trioxide aggregate-induced odontogenic differentiation of dental pulp cells *via* activation of the Wnt/β-catenin signaling pathway. *Journal of Endodontics*, 2016, **42(7):** 1062.

[14] SADEGHZADE S, EMADI R, TAVANGARIAN F. Combustion assisted synthesis of hardystonite nanopowder. *Ceramics International*, 2016, **42(13):** 14656.

[15] SHIE M Y, CHIANG W H, CHEN I W P, *et al.* Synergistic acceleration in the osteogenic and angiogenic differentiation of human mesenchymal stem cells by calcium silicate-graphene composites. *Materials Science and Engineering: C*, 2017, **73:** 726.

[16] DU Z Y, LENG H J, GUO L Y, *et al.* Calcium silicate scaffolds promoting bone regeneration *via* the doping of Mg^{2+} or Mn^{2+} ion. *Composites Part B-Engineering*, 2020, **190:** 15.

[17] VENKATRAMAN S K, SWAMIAPPAN S. Synthesis, bioactivity and mechanical stability of Mg/Ca silicate biocomposites developed for tissue engineering applications. *ChemistrySelect*, 2019, **4(45):** 13099.

[18] ZHU T L, ZHU M, ZHU Y F. Fabrication of forsterite scaffolds with photothermal-induced antibacterial activity by 3D printing and polymer-derived ceramics strategy. *Ceramics International*, 2020, **46(9):** 13607.

[19] LIAO F, PENG X Y, YANG F, *et al.* Gadolinium-doped mesoporous calcium silicate/chitosan scaffolds enhanced bone regeneration

ability. *Materials Science and Engineering: C*, 2019, **104:** 11.

[20] SU Y H, PAN C T, TSENG Y S, *et al.* Rare earth element cerium substituted Ca-Si-Mg system bioceramics: from mechanism to mechanical and degradation properties. *Ceramics International*, 2021, **47(14):** 19414.

[21] KRESSE G, FURTHMULLER J. Efficient iterative schemes for *ab initio* total-energy calculations using a plane-wave basis set. *Physical Review B*, 1996, **54(16):** 11169.

[22] BLOCHL P E. Projector augmented-wave method. *Physical Review B*, 1994, **50(24):** 17953.

[23] BLOCHL P E, JEPSEN O, ANDERSEN O K. Improved tetrahederon method for brillouin-zone integrations. *Physical Review B*, 1994, **49(23):** 16223-16233.

[24] PERDEW J P, BURKE K, ERNZERHOF M. Generalized gradient approximation made simple. *Physical Review Letters*, 1997, **78(7):** 1396.

[25] MONKHORST H J, PACK J D. Special points for brillouin-zone integrations. *Physical Review B*, 1976, **13(12):** 5188.

[26] MOMMA K, IZUMI F. VESTA 3 for three-dimensional visualization of crystal, volumetric and morphology data. *Journal of Applied Crystallography*, 2011, **44:** 1272.

[27] REGI M V, ESBRIT P, SALINAS A J. Degradative effects of the biological environment on ceramic biomaterials. *Biomaterials Science (Fourth Edition)*, 2020**:** 955.

[28] ZHANG M, ZHAI W, CHANG J. Preparation and characterization of a novel willemite bioceramic. *Journal of Materials Science-Materials in Medicine*, 2010, **21(4):** 1169.

[29] DEKOCK R L. Proton affinity and frontier orbital concept-predictions and pitfalls. *Journal of the American Chemical Society*, 1975, **97(19):** 5592.

[30] DEKOCK R L, BARBACHYN M R. Proton affinity, ionization-energy, and the nature of frontier orbital electron-density. *Journal of the American Chemical Society*, 1979, **101(22):** 6516.

[31] HUANG J, WANG B, YU Y, *et al.* Electronic origin of doping-induced enhancements of reactivity: case study of tricalcium silicate. *Journal of Physical Chemistry C*, 2015, **119(46):** 25991.

[32] WU C T, CHANG J. Silicate bioceramics for bone tissue regeneration. *Journal of Inorganic Materials*, 2013, **28(1):** 29.

[33] WU C T, RAMASWAMY Y, BOUGHTON P, *et al.* Improvement of mechanical and biological properties of porous $CaSiO_3$ scaffolds by poly(*D*,*L*-lactic acid) modification. *Acta Biomaterialia*, 2008, **4(2):** 343.

[34] WANG G C, LU Z F, DWARTE D, *et al.* Porous scaffolds with tailored reactivity modulate *in-vitro* osteoblast responses. *Materials Science and Engineering: C*, 2012, **32(7):** 1818.

[35] RAMASWAMY Y, WU C, VAN HUMMEL A, *et al.* The responses of osteoblasts, osteoclasts and endothelial cells to zirconium modified calcium-silicate-based ceramic. *Biomaterials*, 2008, **29(33):** 4392.

[36] GOU Z G, CHANG J, ZHAI W Y, *et al.* Study on the self-setting property and the *in vitro* bioactivity of *β*-Ca_2SiO_4. *Journal of Biomedical Materials Research Part B: Applied Biomaterials*, 2005, **73B(2):** 244.

[37] ZHAO W Y, WANG J Y, ZHAI W Y, *et al.* The self-setting properties and *in vitro* bioactivity of tricalcium silicate. *Biomaterials*, 2005, **26(31):** 6113.

[38] NAJAFINEZHAD A, ABDELLAHI M, GHAYOUR H, *et al.* A comparative study on the synthesis mechanism, bioactivity and mechanical properties of three silicate bioceramics. *Materials Science and Engineering: C*, 2017, **72:** 259.

[39] WANG G C, LU Z F, LIU X Y, *et al.* Nanostructured glass-ceramic coatings for orthopaedic applications. *Journal of the Royal Society Interface*, 2011, **8(61):** 1192.

[40] LI H C, WANG D G, CHEN C Z. Effect of sodium oxide and magnesia on structure, *in vitro* bioactivity and degradability of wollastonite. *Materials Letters*, 2014, **135:** 237.

[41] KALANTARI E, NAGHIB S M, NAIMI-JAMAL M R, *et al.* Nanostructured monticellite for tissue engineering applications — Part I: microstructural and physicochemical characteristics. *Ceramics International*, 2018, **44(11):** 12731.

[42] MA J, HUANG B X, ZHAO X C, *et al. In vitro* degradability and apatite-formation ability of monticellite ($CaMgSiO_4$) bioceramic. *Ceramics International*, 2019, **45(3):** 3754.

[43] RAFIENIA M, BIGHAM A, SAUDI A, *et al.* Gehlenite nanobioceramic: Sol-Gel synthesis, characterization, and *in vitro* assessment of its bioactivity. *Materials Letters*, 2018, **225:** 89.

[44] LU W H, DUAN W, GUO Y P, *et al.* Mechanical properties and *in vitro* bioactivity of $Ca_5(PO_4)_2SiO_4$ bioceramic. *Journal of Biomaterials Applications*, 2012, **26(6):** 637.

[45] TAVANGARIAN F, EMADI R. Nanostructure effects on the bioactivity of forsterite bioceramic. *Materials Letters*, 2011, **65(4):** 740.

[46] SUN H, HE S W, WU P, *et al.* A novel MgO-CaO-SiO_2 system for fabricating bone scaffolds with improved overall performance. *Materials*, 2016, **9(4):** 12.

[47] JIN X G, CHANG J A, ZHAI W Y, *et al.* Preparation and characterization of clinoenstatite bioceramics. *Journal of the American Ceramic Society*, 2011, **94(1):** 173.

[48] ZHAO Y K, NING C Q, CHANG J. Sol-Gel synthesis of Na_2CaSiO_4 and its *in vitro* biological behaviors. *Journal of Sol-Gel Science and Technology*, 2009, **52(1):** 69.

[49] DU R L, CHANG J. Preparation and characterization of bioactive sol-gel-derived $Na_2Ca_2Si_3O_9$. *Journal of Materials Science-Materials in Medicine*, 2004, **15(12):** 1285.

[50] ZHANG M L, WU C T, LIN K L, *et al.* Biological responses of human bone marrow mesenchymal stem cells to Sr-M-Si (M = Zn, Mg) silicate bioceramics. *Journal of Biomedical Materials Research Part A*, 2012, **100A(11):** 2979.

[51] ZHANG M L, LIN K L, CHANG J. Preparation and characterization of Sr-hardystonite ($Sr_2ZnSi_2O_7$) for bone repair applications. *Materials Science and Engineering: C*, 2012, **32(2):** 184.

[52] ZHANG M L, ZHAI W Y, LIN K L, *et al.* Synthesis, *in vitro* hydroxyapatite forming ability, and cytocompatibility of strontium silicate powders. *Journal of Biomedical Materials Research Part B: Applied Biomaterials*, 2010, **93B(1):** 252.

[53] ZHANG M L, ZHAI W Y, CHANG J. Preparation and characterization of a novel willemite bioceramic. *Journal of Materials Science-Materials in Medicine*, 2010, **21(4):** 1169.

[54] XU H Y, ZHAI D, CAO W T, *et al.* Mineralization activity of $Li_2Ca_2Si_2O_7$ bioceramics. *Journal of Inorganic Materials*, 2021, **36(7):** 753.

[55] WANG X, CHANG J. Application of bioceramics in tissue engineering. *Chinese Bulletin of Life Sciences*, 2020, **32(3):** 257.

[56] KUCKO N W, HERBER R P, LEEUWENBURGH S C G, *et al.* Calcium phosphate bioceramics and cements. //ANTHONY A, ROBERT L, TONY M, ROBERT N, *et al.* Principles of Regenerative Medicine (Third Edition). New York: Academic Press, 2019**:** 591.

[57] DOROZHKIN S V. Calcium orthophosphate bioceramics. *Ceramics International*, 2015, **41(10):** 13913.

[58] HABIBOVIC P, BASSETT D C, DOILLON C J, *et al.* Collagen

biomineralization *in vivo* by sustained release of inorganic phosphate ions. *Advanced Materials*, 2010, **22(16):** 1858.
[59] MA H, FENG C, CHANG J, *et al.* 3D-printed bioceramic scaffolds: from bone tissue engineering to tumor therapy. *Acta Biomaterialia*, 2018, **79:** 37.
[60] NABIYOUNI M, BRÜCKNER T, ZHOU H, *et al.* Magnesium-based bioceramics in orthopedic applications. *Acta Biomaterialia*, 2018, **66:** 23.

基于 DFT 的描述符预测生物陶瓷的降解性

陈梦杰[1,2], 王倩倩[1,2], 吴成铁[1,2], 黄 健[1,2,3]

(1. 中国科学院 上海硅酸盐研究所 高性能陶瓷和超微结构国家重点实验室, 上海 200050; 2. 中国科学院大学 材料科学与光电技术中心, 北京 100049; 3. 上海大学 材料基因组工程研究院, 上海 200444)

摘 要: 生物陶瓷以其优异的生物活性和可降解性在骨缺损修复领域受到广泛关注。然而, 如何使生物陶瓷降解速率与新骨生成速率相匹配仍然存在挑战, 因此需要更深入地了解生物陶瓷的降解特性。本研究采用密度泛函理论(DFT)计算并探索硅酸盐生物陶瓷的电子结构。研究结果表明硅酸盐生物陶瓷价带顶电荷密度的最大值(VBM_{Fmax})与其降解性之间存在线性相关性, 随后的降解实验验证了这种相关性。此外, 对磷酸盐生物陶瓷的研究也证实了该描述符可用于预测不同生物陶瓷的降解性。这一发现有助于更好地理解生物陶瓷的降解机制, 并有望加速可控降解生物陶瓷的设计和开发。

关 键 词: 生物陶瓷; 硅酸盐; 磷酸盐; 第一性原理; 降解

中图分类号: TQ174 **文献标志码:** A **文章编号:** 1000-324X(2024)10-1175-07

Supporting materials:

Predicting the Degradability of Bioceramics through a DFT-based Descriptor

CHEN Mengjie[1,2], WANG Qianqian[1,2], WU Chengtie[1,2], HUANG Jian[1,2,3]

(1. State Key Laboratory of High Performance Ceramics and Superfine Microstructure, Shanghai Institute of Ceramics, Chinese Academy of Sciences, Shanghai 200050, China; 2. Center of Materials Science and Optoelectronics Engineering, University of Chinese Academy of Sciences, Beijing 100049, China; 3. Materials Genome Institute, Shanghai University, Shanghai 200444, China)

Table S1 Structural properties of silicate bioceramics

Bioceramic		*a*/Å	*b*/Å	*c*/Å	*α*/(°)	*β*/(°)	*γ*/(°)	Cell volume/Å^3	Density/ (g·cm^{-3})	Void space/%
α-$CaSiO_3$	Calc.	11.9532	6.9367	10.6153	90	111.274	90	820.198	2.8224	58.32
	Expt.	11.8322	6.8624	10.5297	90	111.245	90	796.878	N/A	N/A
β-$CaSiO_3$	Calc.	8.0250	7.3910	7.1500	90.083	95.531	103.437	410.433	2.8201	58.03
	Expt.	7.9400	7.3200	7.0700	90.030	95.370	103.430	397.818	N/A	N/A
Ca_2SiO_4	Calc.	5.1234	11.3455	6.8071	90	90	90	395.748	2.8910	57.19
	Expt.	5.0910	11.3710	6.7820	90	90	90	392.608	N/A	N/A
Ca_3SiO_5	Calc.	11.7501	14.3209	13.7622	104.813	94.354	90.117	2231.821	3.0580	54.91
	Expt.	11.6700	14.2400	13.7200	105.500	94.330	90	2190.324	N/A	N/A
$Ca_2MgSi_2O_7$	Calc.	7.9073	7.9073	5.053	90	90	90	315.940	2.8661	57.30
	Expt.	7.8900	7.8900	5.0410	90	90	90	313.813	N/A	N/A
$Ca_2ZnSi_2O_7$	Calc.	7.9043	7.9043	5.0592	90	90	90	316.089	3.2961	57.87
	Expt.	7.8279	7.8279	5.0138	90	90	90	307.226	N/A	N/A
$Ca_3MgSi_2O_8$	Calc.	9.8453	5.2925	13.7871	90	97.954	90	711.477	3.0690	54.41
	Expt.	9.9678	5.2693	13.6701	90	97.720	90	711.498	N/A	N/A
$Ca_3ZrSi_2O_9$	Calc.	7.4323	10.3145	10.5148	90	91.113	90	805.919	3.3927	56.03
	Expt.	7.3603	10.1766	10.4514	90	90.875	90	782.748	N/A	N/A
$CaMgSi_2O_6$	Calc.	9.8690	9.0131	5.3152	90	106.122	90	454.197	3.1672	52.58
	Expt.	9.7760	8.9790	5.2670	90	105.940	90	444.554	N/A	N/A
$CaMgSiO_4$	Calc.	5.2260	6.8631	9.1738	90	90	90	327.740	3.1714	52.65
	Expt.	5.2408	6.8696	9.1348	90	90	90	328.869	N/A	N/A
$CaTiSiO_5$	Calc.	7.1294	8.7726	6.6609	90	114.041	90	380.457	3.4231	53.08
	Expt.	7.0730	8.7180	6.5550	90	113.970	90	369.339	N/A	N/A
$Ca_2Al_2SiO_7$	Calc.	7.6773	7.6773	5.1888	90	90	90	305.833	2.9777	56.92
	Expt.	7.6764	7.6764	5.1908	90	90	90	305.878	N/A	N/A
$Ca_5(PO_4)_2SiO_4$	Calc.	6.8737	10.2116	15.4913	90	90	90	1087.357	2.9470	55.64
	Expt.	6.7370	10.1320	15.5080	90	90	90	1058.565	N/A	N/A
Mg_2SiO_4	Calc.	4.8043	10.3245	6.0475	90	90	90	299.970	3.1157	52.95
	Expt.	4.7630	10.2400	5.9990	90	90	90	292.590	N/A	N/A
$MgSiO_3$	Calc.	9.3655	8.8559	5.3797	90	90	90	446.190	2.9892	54.83
	Expt.	9.2500	8.7400	5.3200	90	90	90	430.095	N/A	N/A
Na_2CaSiO_4	Calc.	7.5297	7.5297	7.5297	90	90	90	426.904	2.7719	53.91
	Expt.	7.4800	7.4800	7.4800	90	90	90	418.509	N/A	N/A
$Na_2Ca_2Si_3O_9$	Calc.	10.6053	10.6053	13.3064	89.839	90.161	120.224	1293.145	2.7306	58.66
	Expt.	10.5989	10.5989	13.3074	89.720	90.280	120.203	1291.944	N/A	N/A
$Sr_2MgSi_2O_7$	Calc.	8.0962	8.0962	5.2249	90	90	90	342.478	3.5660	56.58
	Expt.	8.0107	8.0107	5.1636	90	90	90	331.355	N/A	N/A
$Sr_2ZnSi_2O_7$	Calc.	8.0954	8.0954	5.2322	90	90	90	342.897	3.9593	57.16
	Expt.	8.0007	8.0007	5.1722	90	90	90	331.079	N/A	N/A
$SrSiO_3$	Calc.	12.4873	7.2366	10.9917	90	111.645	90	923.231	3.5335	58.61
	Expt.	12.3330	7.1460	10.8850	90	111.570	90	892.131	N/A	N/A
Zn_2SiO_4	Calc.	14.1481	14.1481	9.4163	90	90	120	1632.331	4.0803	63.23
	Expt.	13.9710	13.9710	9.3340	90	90	120	1577.805	N/A	N/A
$Li_2Ca_2Si_2O_7$	Calc.	5.1459	5.1459	41.6617	90	90	120	955.403	2.7346	57.34
	Expt.	5.1471	5.1471	41.6291	90	90	120	955.116	N/A	N/A

Table S2　Summary of degradation studies for silicate bioceramics

Bioceramic	Surrounding aqueous media	Weight loss	Total ion release in media after 7 d
α-$CaSiO_3$	SBF	31.27% (28 d)	N/A
	SBF	16.58% (28 d)	Ca: ~3.58 mmol·L^{-1}/Si: ~0.67 mmol·L^{-1}
β-$CaSiO_3$	Tris-HCl	24.8% (28 d)	N/A
	SBF	N/A	Ca: ~9.59 mmol·L^{-1}/Si: ~1.73 mmol·L^{-1}
Ca_2SiO_4	SBF	N/A	Ca: ~4.77 mmol·L^{-1}/Si: ~0.83 mmol·L^{-1}
Ca_3SiO_5	SBF	N/A	Ca: ~6.82 mmol·L^{-1}/Si: ~2.20 mmol·L^{-1}
$Ca_2MgSi_2O_7$	Tris-HCl	12.1% (28 d)	(2 d) Ca: ~13.51 mmol·L^{-1}/Si: ~0.26 mmol·L^{-1}/Mg: ~3.49 mmol·L^{-1}
	SBF	N/A	Ca: ~4.50 mmol·L^{-1}/Si: ~2.18 mmol·L^{-1}/Mg: ~2.15 mmol·L^{-1}
	SBF	N/A	Ca: ~2.38 mmol·L^{-1}/Si: ~0.91 mmol·L^{-1}/Mg: ~1.23 mmol·L^{-1}
$Ca_2ZnSi_2O_7$	Tris-HCl	8.4% (28 d)	(2 d) Ca: ~11.10 mmol·L^{-1}/Si: ~0.17 mmol·L^{-1}/Zn: ~0.06 mmol·L^{-1}
	Tris-HCl	N/A	Ca: ~2.68 mmol·L^{-1}/Si: ~0.47 mmol·L^{-1}/Zn: ~0.01 mmol·L^{-1}
	Tris-HCl	3.17% (28 d)	Ca: ~0.55 mmol·L^{-1}/Si: ~0.17 mmol·L^{-1}/Zn: ~0.02 mmol·L^{-1}
$Ca_3MgSi_2O_8$	Tris-HCl	3.05% (7 d)	N/A
$Ca_3ZrSi_2O_9$	SBF	N/A	Ca: ~2.55 mmol·L^{-1}/Si: ~1.52 mmol·L^{-1}/Zr: ~0.43 mmol·L^{-1}
	SBF	N/A	Ca: ~9.15 mmol·L^{-1}/Si: ~1.55 mmol·L^{-1}
$CaMgSi_2O_6$	SBF	N/A	Ca: ~3.87 mmol·L^{-1}/Si: ~1.95 mmol·L^{-1}/Mg: ~2.01 mmol·L^{-1}
	SBF	N/A	Ca: ~1.75 mmol·L^{-1}/Si: ~1.11 mmol·L^{-1}/Mg: ~0.85 mmol·L^{-1}
$CaMgSiO_4$	SBF	N/A	Ca: ~7.00 mmol·L^{-1}/Si: ~2.64 mmol·L^{-1}/Mg: ~3.29 mmol·L^{-1}
	SBF	2.07% (7 d) 3.51% (14 d) 6.92% (28 d)	(2 d) Ca: ~13.17 mmol·L^{-1}/Si: ~0.06 mmol·L^{-1}/Mg: ~4.33 mmol·L^{-1}
$CaTiSiO_5$	Tris-HCl	N/A	Ca: ~0.23 mmol·L^{-1}/Si: ~0.05 mmol·L^{-1}
$Ca_2Al_2SiO_7$	SBF	N/A	Ca: ~2.64 mmol·L^{-1}/Si: ~0.21 mmol·L^{-1}/Al: ~0.12 mmol·L^{-1}
$Ca_5(PO_4)_2SiO_4$	SBF	N/A	Ca: ~7.10 mmol·L^{-1}/Si: ~3.88 mmol·L^{-1}/P: ~1.58 mmol·L^{-1}
Mg_2SiO_4	SBF	N/A	Ca: ~1.52 mmol·L^{-1}/Mg: ~2.78 mmol·L^{-1}
	PBS	0.11% (28 d)	N/A
$MgSiO_3$	Tris-HCl	7.31% (7 d) 10.77% (14 d)	N/A
Na_2CaSiO_4	PBS / SBF	2.49% (7 d) 2.86% (14 d) 1.72% (28 d)	Ca: ~5.68 mmol·L^{-1}/Si: ~0.46 mmol·L^{-1}
$Na_2Ca_2Si_3O_9$	Tris-HCl	4.32% (7 d)	N/A
	SBF	N/A	Ca: ~4.98/Si: ~0.87/Na: 172.57 (×10^{-6} mmol·L^{-1})
$Sr_2MgSi_2O_7$	N/A	N/A	(14 d) Sr: ~1.70 mmol·L^{-1}/Si: ~2.24 mmol·L^{-1} / Mg: ~1.97 mmol·L^{-1}
$Sr_2ZnSi_2O_7$	N/A	N/A	(14 d) Sr: ~1.71 mmol·L^{-1}/Si: ~0.97 mmol·L^{-1} / Zn: ~0.024 mmol·L^{-1}
	Tris-HCl	1.19% (7 d) 1.70% (14 d) 2.26% (28 d)	N/A
$SrSiO_3$	SBF	N/A	Sr: ~8.27 mmol·L^{-1}/Si: ~2.35 mmol·L^{-1}
Zn_2SiO_4	N/A	N/A	Zn: ~0.012 mmol·L^{-1}/Si: ~0.015 mmol·L^{-1}
$Li_2Ca_2Si_2O_7$	SBF	N/A	Ca: ~3.12 mmol·L^{-1}/Si: ~2.33 mmol·L^{-1}/Li: ~0.82 mmol·L^{-1}

Table S3 Summary of degradation studies for phosphate bioceramics

Ca (Mg)/P molar ratio	Compounds and their typical abbreviations	Chemical formula	Solubility at 25 ℃ in SBF/(g·L^{-1})
1.0	Dicalcium phosphate anhydrous (DCPA or DCP), mineral monetite	$CaHPO_4$	~0.048
1.33	Octacalcium phosphate (OCP)	$Ca_8(HPO_4)_2(PO_4)_4·5H_2O$	~0.0081
1.5	α-Tricalcium phosphate(α-TCP)	α-$Ca_3(PO_4)_2$	~0.0025
1.5	β-Tricalcium phosphate(β-TCP)	β-$Ca_3(PO_4)_2$	~0.0005
1.67	Hydroxyapatite (HA or HAP)	$Ca_{10}(PO_4)_6(OH)_2$	~0.0003
1.67	Fluorapatite (FA or FAP)	$Ca_{10}(PO_4)_6F_2$	~0.0002
1.67	Oxyapatite (OA、OAP or OXA), mineral voelckerite	$Ca_{10}(PO_4)_6O$	~0.087
1.5	Farringtonite	$Mg_3(PO_4)_2$	~0.00215
1.5	Bobierrite	$Mg_3(PO_4)_2·8H_2O$	~0.0062
1.5	Cattiite	$Mg_3(PO_4)_2·22H_2O$	~0.00146

Table S4 Structural properties of phosphate bioceramics

Bioceramic		*a*/Å	*b*/Å	*c*/Å	*α*/(°)	*β*/(°)	*γ*/(°)	Cell volume/Å^3	Density/(g·cm^{-3})	Void space/%
DCP	Calc.	6.7222	6.9771	7.1003	75.727	83.353	88.127	320.567	2.8192	55.11
	Expt.	6.7205	6.9810	7.0970	75.716	83.359	88.176	320.503	N/A	N/A
OCP	Calc.	20.0539	9.6632	6.9266	90.376	93.188	110.180	1257.459	2.5951	58.04
	Expt.	19.6920	9.5230	6.8350	90.150	92.540	108.650	1213.058	N/A	N/A
α-TCP	Calc.	5.2650	5.2650	7.2297	89.964	90.036	64.657	181.125	2.8437	57.68
	Expt.	5.2719	5.2719	7.2338	89.713	90.287	64.441	181.367	N/A	N/A
β-TCP	Calc.	14.1827	14.1827	14.1827	43.823	43.823	43.823	1241.876	2.9033	75.04
	Expt.	14.4070	14.4070	14.4070	43.443	43.443	43.443	1282.726	N/A	N/A
HAP	Calc.	9.5609	9.5609	6.9081	90	90	120	546.872	3.0505	55.17
	Expt.	9.4240	9.4240	6.8790	90	90	120	529.086	N/A	N/A
FAP	Calc.	9.5015	9.5015	6.9174	90	90	120	540.833	3.0968	54.78
	Expt.	9.3770	9.3770	6.8880	90	90	120	524.507	N/A	N/A
OAP	Calc.	9.6140	9.6140	6.8905	90	90	120	551.555	2.9704	56.88
	Expt.	9.4320	9.4320	6.8810	90	90	120	530.139	N/A	N/A
$Mg_3(PO_4)_2$	Calc.	5.1226	8.3405	8.9544	90	120.550	90	329.469	2.6498	60.83
	Expt.	5.1224	8.3404	8.9544	90	120.549	90	329.456	N/A	N/A
$Mg_3(PO_4)_2·8H_2O$	Calc.	8.4348	8.4348	4.6912	80.689	99.311	74.357	309.660	2.1825	59.26
	Expt.	8.4235	8.4235	4.6942	80.788	99.212	74.232	309.059	N/A	N/A
$Mg_3(PO_4)_2·22H_2O$	Calc.	6.8362	7.0170	15.8842	87.185	94.670	118.362	668.225	1.6382	66.59
	Expt.	6.9265	7.0204	15.9613	88.374	94.305	119.386	674.334	N/A	N/A